Supplemental Material

Table S1. Baseline Internal Diameter at 60 cm H_20 (number of vessels)

Group	Diameter
FVB WT	142.0 ± 6.1 (5)
Apoe$^{-/-}$	143.3 ± 9.0 (7)
Apoe$^{-/-}$ + MβCD	143.5 ± 11.9 (3)
Kir2.1$^{+/-}$/*Apoe*$^{-/-}$	146.9 ± 8.5 (13)
Kir2.1$^{+/-}$/*Apoe*$^{-/-}$ + MβCD	148.74 ± 12.2 (5)
Kir2.1$^{+/-}$	131.7 ± 8.2 (7)
B6 WT	132.8 ± 17.1 (5)
Apoe$^{-/-}$	149.9 ± 14.5 (9)
FVB *Apoe*$^{-/-}$	
Empty-AV	90.8 ± 13.6 (4)
WT Kir2.1-AV	123.5 ± 8.2 (4)
B6 HFD *Apoe*$^{-/-}$	
Empty-AV	122.4 ± 13.1 (8)
WT Kir2.1-AV	128.1 ± 20.8 (4)
DN Kir2.1-AV	130.7 ± 11.1 (4)

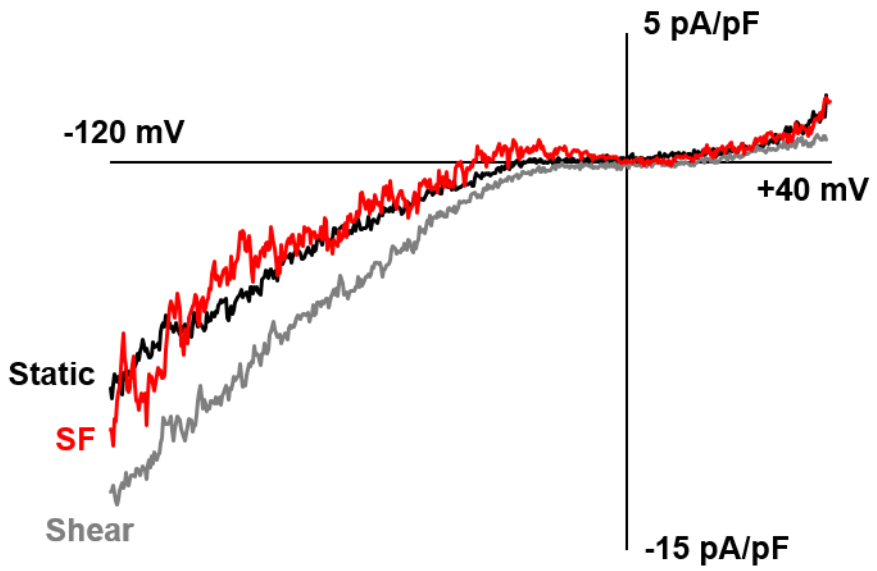

Figure S1. Stopping flow returns currents to static baseline and acLDL. Representative perforated patch recording showing static Kir currents (black), shear stress (0.7 dynes/cm^2)-induced activation of Kir currents using the gravity perfused minimally invasive flow (MIF) device (gray), and the return to static Kir currents upon stopping flow (SF) to the MIF device (red). A voltage ramp from -120 to +40 mV was used to elicit inwardly rectifying K^+ current in a 60 mM K^+ bath (E_K ~ -20 mV).

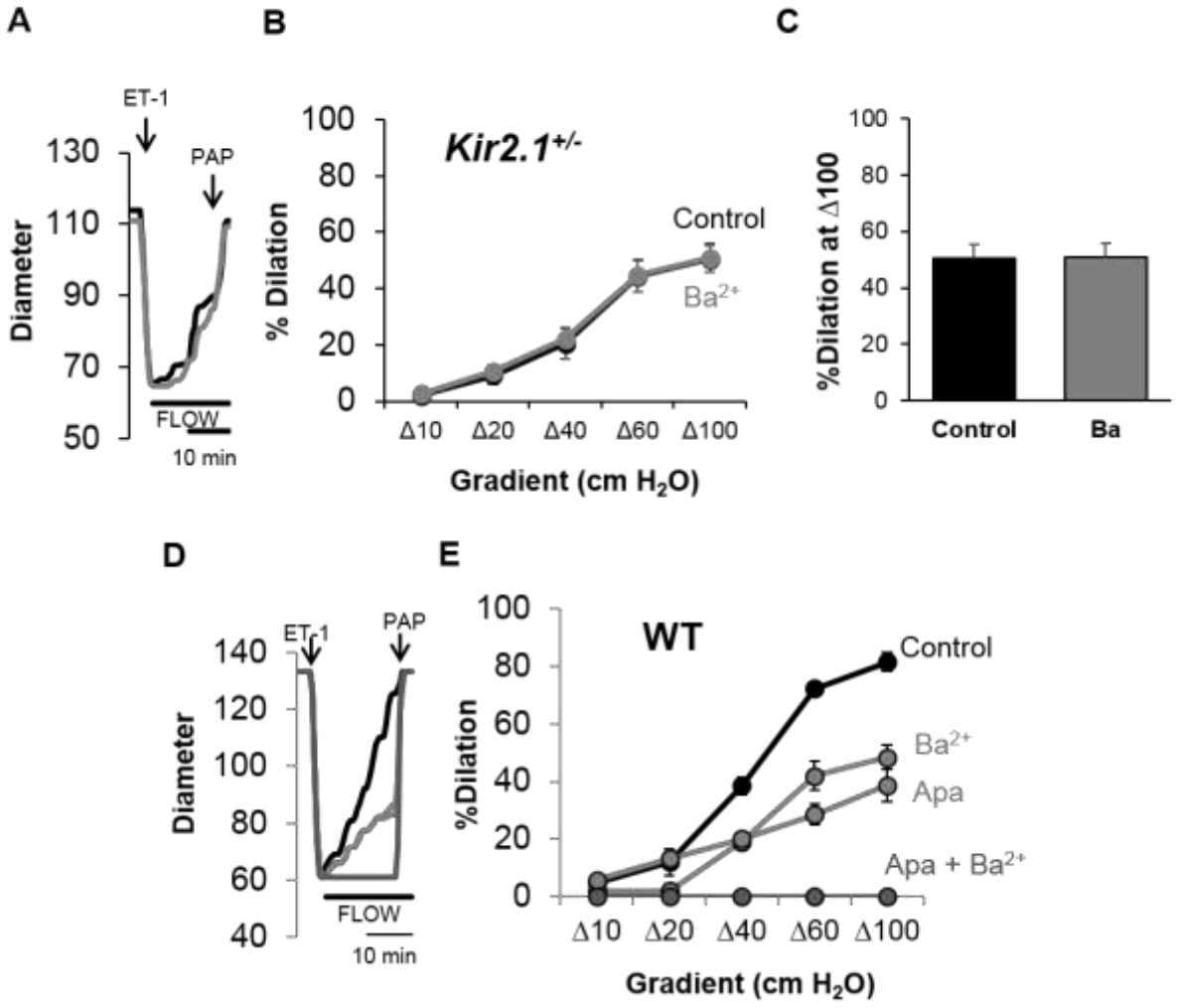

Figure S2. Mesenteric arteries from *Kir2.1*$^{+/-}$ exhibit reduced, Ba^{2+}-insensitive dilations to flow. Representative flow-induced vasodilation (FIV) traces from A) *Kir2.1*$^{+/-}$ and D) WT mice generated using the pressure gradient method to induce intraluminal flow through mesenteric arteries. Endothelin-1 (ET-1) (1.2-2 x 10^{-10} mol/L) was used to pre-constrict arteries and papaverine (10^{-4} mol/L) was used to test arterial function at the end of each protocol. FIV curves from B) *Kir2.1*$^{+/-}$ and E) WT mice show the differences in Ba^{2+} (3 x 10^{-5} mol/L) sensitivity. Furthermore, FIV in WT mice is sensitive to apamin (2 x 10^{-8} mol/L) and abolished by the combination of Ba^{2+} and apamin. C) *Kir2.1+/-* group data highlighting FIV before (control) and after application of Ba^{2+} measured at Δ100 cm H_2O. n = 6 arteries from 4 mice for both WT and *Kir2.1*$^{+/-}$ groups. All error bars represent SEM which was calculated using n = number of mice.

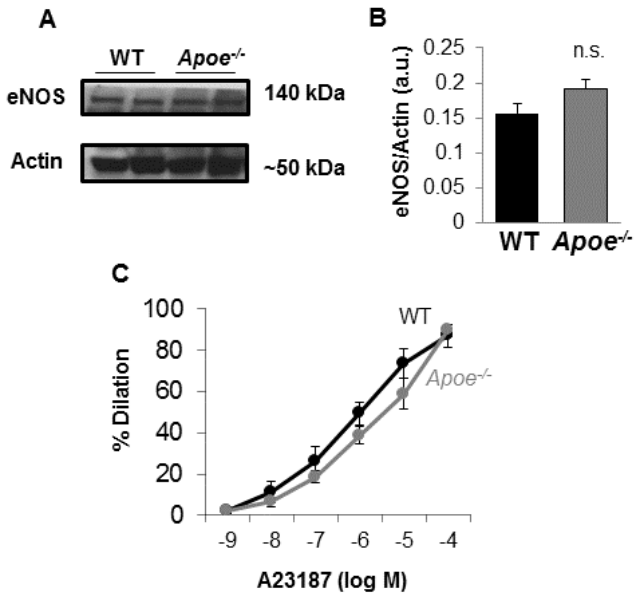

Figure S3. eNOS expression and function are intact in *Apoe*$^{-/-}$ mice. A) Representative Western blot showing total endothelial nitric oxide synthase (eNOS) expression in whole mesenteric arcades from WT and *Apoe*$^{-/-}$ mice and B) group data normalized to actin expression (n = 4). C) No differences were observed in eNOS functional capacity as measured in arteries isolated from WT (n = 6 arteries from 3 mice) and *Apoe*$^{-/-}$ (n = 9 arteries from 5 mice) mice using a dose-response to the Ca^{2+} ionophore, A23187. In all cases, SEM is calculated as n = number of mice.

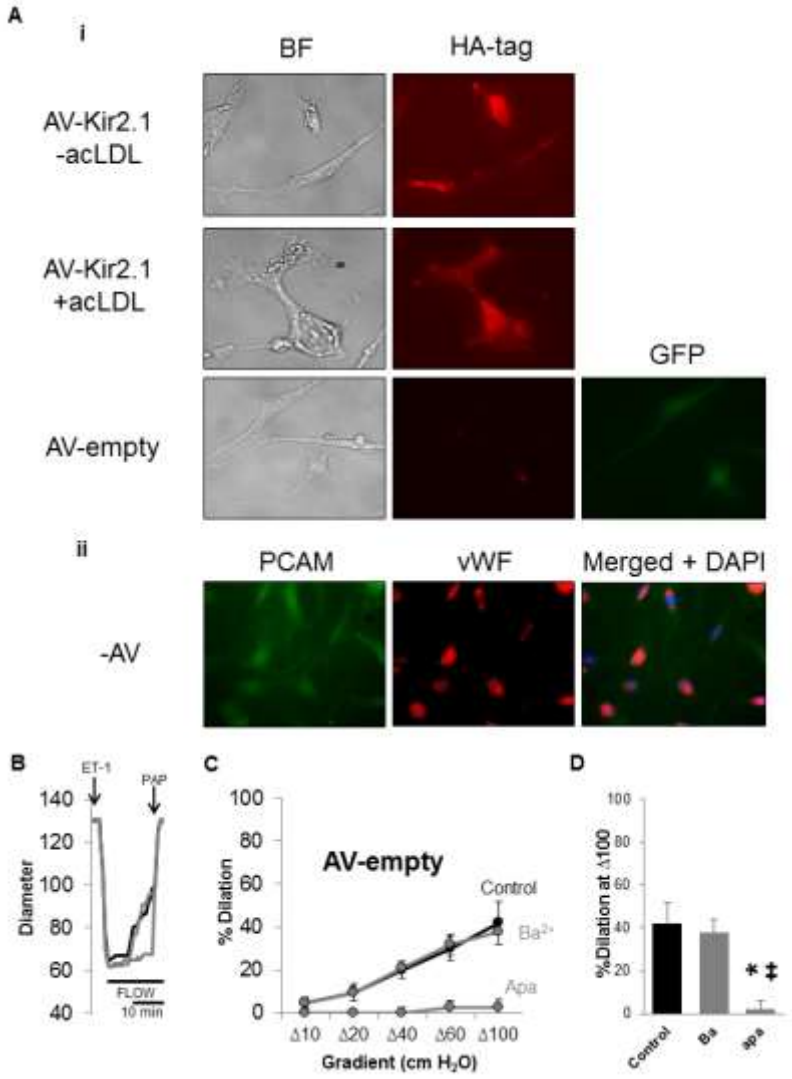

Figure S4. Incubating ECs with acLDL does not prevent adenoviral overexpression of Kir2.1 and empty AV transduction has no effect on FIV in *Apoe*$^{-/-}$ mice. Ai) Endothelial cells (ECs) transduced with adenovirus (AV)-Kir2.1 show detectable hematgglutinin (HA)-tag fluorescence in the presence (middle panel) or absence (top panel) of acetylated low density lipoprotein (acLDL, 50 µg/ml; 24 hour incubation). HA-tag fluorescence was not detected in those ECs transduced with AV-empty (bottom panel), however, GFP fluorescence is observed to indicate successful transduction of cells. Considerable changes in morphology were observed with adenoviral transduction, therefore, we show Aii) photomicrographs confirming the appropriate morphology and expected staining of cultured ECs by PCAM (left) and Von Willebrand factor (middle) in non-transduced ECs in culture. B) Representative flow-induced vasodilation (FIV) trace from a mesenteric artery transduced with AV-empty. Endothelin-1 (ET-1) and papaverine were used as described above. C) FIV curves show that AV-empty transduction has no effect on *Apoe*$^{-/-}$ response to flow. D) Group data highlighting the dilations to flow at Δ100 cm H_2O. Only apamin (2 x 10^{-8} mol/L) inhibits FIV in *Apoe*$^{-/-}$ arteries transduced with AV-empty (n = 4). **P* < 0.05 vs. control, ‡*P* < 0.05 vs. Ba^{2+} (3 x 10^{-5} mol/L). Error bars represent SEM.

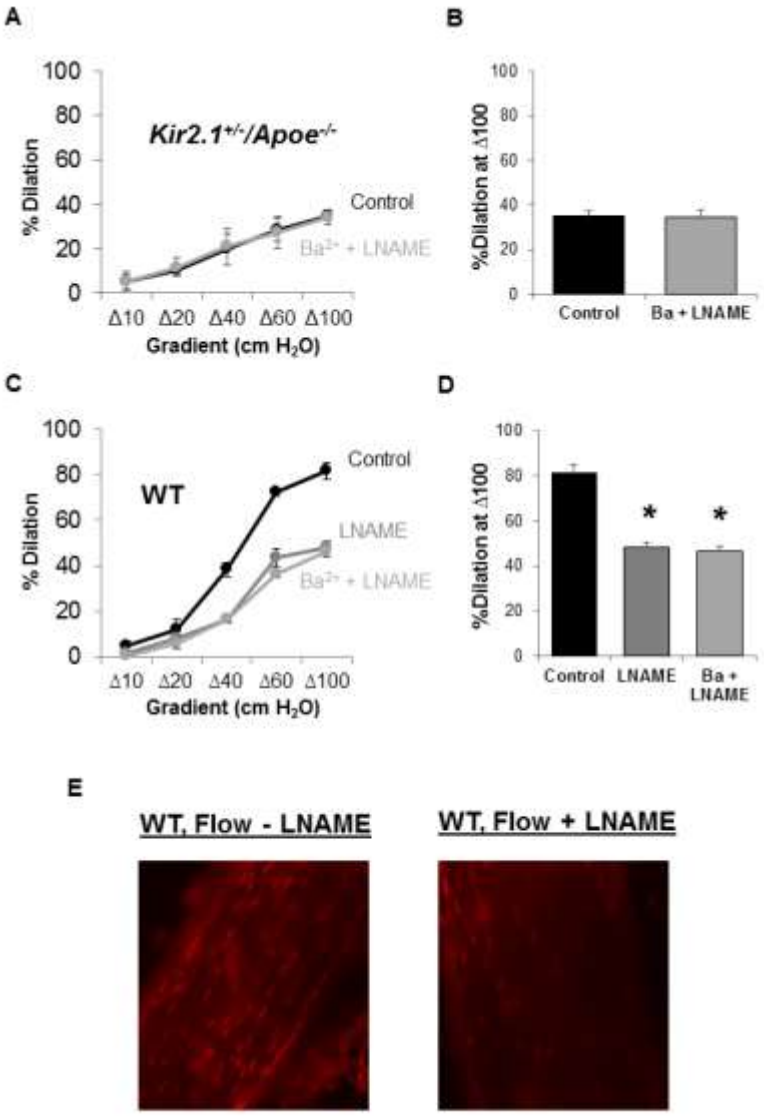

Figure S5. The effect of LNAME on FIV in arteries from *Kir2.1*$^{+/-}$*/Apoe*$^{-/-}$ and WT mice. Flow-induced vasodilation (FIV) curves generated from A) *Kir2.1*$^{+/-}$*/Apoe*$^{-/-}$ and C) WT mesenteric arteries and exposed to either L-N^{G}-Nitroarginine methyl ester (LNAME, 10^{-4} mol/L) or a combination of Ba^{2+} (3 x 10^{-5} mol/L) and LNAME. Group data highlighting dilations to flow at Δ100 cm H_2O in B) *Kir2.1*$^{+/-}$*/Apoe*$^{-/-}$ (n = 4 arteries from 4 mice) and D) WT mice (n = 6 arteries from 4 mice). **P* < 0.05 vs. control. Error bars represent SEM which was calculated as n = number of mice. E) Representative images providing good positive controls for the detection of nitric oxide (NO) via the dye Diaminorhodamine-4M (DAR4M). Arteries from WT mice exposed to intraluminal flow (Δ60 for 30 minutes) have robust NO production (left) that is prevented by incubating arteries with LNAME (10^{-4} mol/L, right) for 20 minutes prior to and during intraluminal flow (Δ60 for 30 minutes).

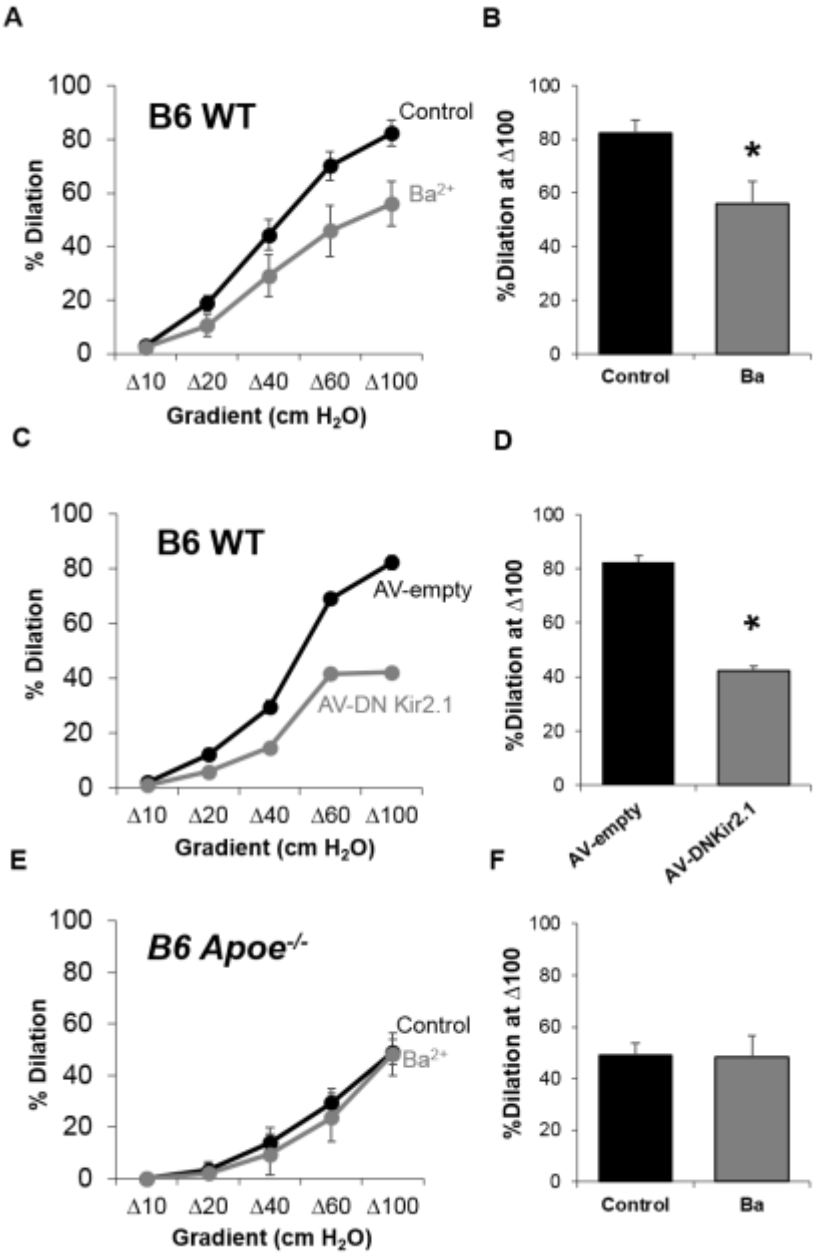

Figure S6. Endothelial Kir2.1 is a major contributor to FIV in mesenteric arteries from C57BL/6 (B6) mice. FIV curves generated from C57/BL6 (B6) WT mice reveal sensitivity to A) Ba^{2+} (3 x 10^{-5} mol/L; n = 5 arteries from 4 mice), and C) transduction with endothelial specific adenovirus (AV)-dominant negative (DN) Kir2.1 (n = 4 pairs of arteries from 4 mice). E) B6 *Apoe*$^{-/-}$ mice (n = 9 arteries from 5 mice), however, lack sensitivity to Ba^{2+}. B, D, F) Group data highlighting the differences in FIV measured at Δ100 cm H_2O for each of A, C, and E, respectively. *P < 0.05 vs. B) control and D) AV-empty. Error bars represent SEM using n = number of mice.

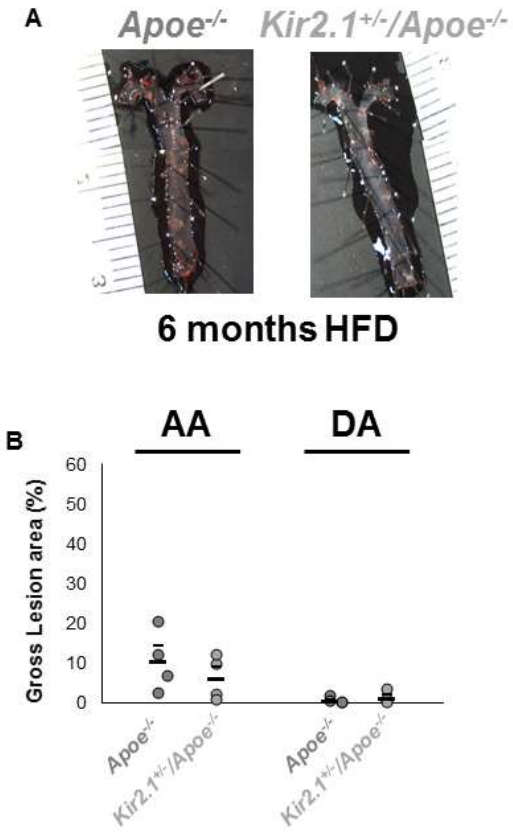

Figure S7. Lesion formation in *Apoe*$^{-/-}$ and *Kir2.1*$^{+/-}$*/Apoe*$^{-/-}$ mice aortas after 6 months of high fat feeding. A) Representative images of *en face* aortas from *Apoe*$^{-/-}$ (left) and *Kir2.1*$^{+/-}$*/Apoe*$^{-/-}$ (right) stained with oil red O for lesion detection. Mice were fed a Western, high fat, high cholesterol diet for 6 months prior to analysis. B) Group analyses of the lesions detected in aortic arch (AA) and descending arch (DA) and measured as percentage of the total area containing lesions in *Apoe*$^{-/-}$ (n = 4) and *Kir2.1*$^{+/-}$*/Apoe*$^{-/-}$ (n = 4). Larger, lower bars represent the group average and smaller, upper bars represent the standard error. No significant differences were found between *Apoe*$^{-/-}$ and *Kir2.1*$^{+/-}$*/Apoe*$^{-/-}$ groups using a two-way ANOVA.